ACADEMIA ROMÂNĂ
Revue Roumaine de Chimie
http://web.icf.ro/rrch/

Rev. Roum. Chim.,
2021, *66*(7), 633–644
DOI: 10.33224/rrch.2021.66.7.06

THEORETICAL STUDY OF CHALCONE DERIVATIVES AS CORROSION INHIBITORS FOR ALUMINUM IN ACIDIC ENVIRONMENT

Wahiba MECIBAH,[a*] Hamza ALLAL,[a,b] Mouna CHERIFI,[c] Souad BOUASLA[d] and Nabila BOUTEMINE[c]

[a] Department of Technology, Faculty of Technology, University August 20, 1955 – Skikda, 21000, Algeria
[b] Research Unit of Environmental Chemistry and Molecular Structural (CHEMS), University of Constantine-1, 25000, Constantine, Algeria
[c] Laboratory of Water Treatment and Valorization of Industrial Wastes, Department of Chemistry, Badji-Mokhtar University, Annaba, Algeria
[d] Department of Chemistry and Physics, Normal High School of Technology Education (ENSET) Skikda, Algeria

Received January 23, 2021

Quantum chemical calculations based on DFT method were performed on three chalcone derivatives (Benzalacetophenone, Dibenzalacetone, Dibenzal-1,4-Diacetylbenzene) used as corrosion inhibitors for aluminum in 1M phosphoric acid media to determine the relationship between the molecular structure and inhibition efficiency. Quantum chemical parameters such as E_{HOMO}, E_{LUMO}, energy gap (ΔE_{gap}), dipole moment (μ), electronegativity (χ), global hardness (η) and fraction of electron transfers (ΔN) from the inhibitor molecule to the aluminum surface have been calculated to investigate their relative corrosion inhibition performances. The local reactivity has been analyzed through the condensed Fukui functions and local softness indices in order to predict the most possible sites for nucleophilic and electrophilic attacks. The effectiveness of the DFT calculations in predicting the inhibition efficiency was proven. The protonation of the studied chalcone molecules was examined and analyzed.

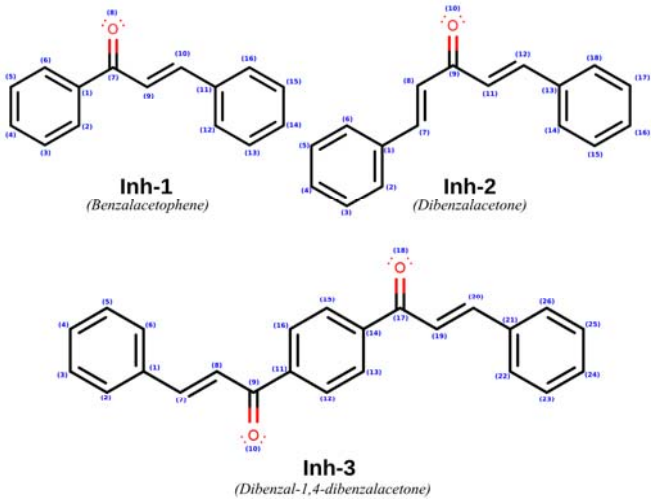

INTRODUCTION

Aluminium and its alloys are of considerable importance, owing to their particular properties such as strength, ductility, formability, workability and good thermal and electrical conductivity. They are extensively used in the industrial sector especially in aviation, aerospace, automotive, military hardware, ship building and household appliances.[1] They are very useful materials due to their good mechanical and physical properties such as their weight-to-high strength ratio, good machining properties, recyclability, and their corrosion resistance.[2] Aluminium resistance is originated from the formation of a thin layer oxide film. However, this film is an insufficient barrier for relatively long-term corrosion protection. This is because aluminium is able to react both as a base or an acid, which means its oxide film is stable in neutral conditions but soluble in acidic and alkaline environments.[3] Despite the huge benefit of Aluminium when compared to other metals, it is

* Corresponding author: mecibahwahiba@yahoo.fr

not always resistant to corrosion, especially in contact with an aggressive solution, during cleaning with hydrochloric acid, acid descaling, chemical and electrochemical etching in many chemical industrial process. Which presents a serious economic issue, hence the importance of using corrosion inhibitors to prevent metal dissolution and minimize acid consumption.[4-7] One of the most effective acid corrosion inhibitors are organic compounds containing nitrogen, oxygen and/or sulfur atoms.[8,9] Electrons interaction between Aluminium d-orbitals and the inhibitor molecule, are facilitated by the presence of π-electrons from multiple bonds or aromatic rings.[5,10] Chalcones are one of the most important classes of flavonoids in plant kingdom.[11] Having a large number of replaceable hydrogens which offers them a wide variety of derivatives as well as a wide spectrum of biological activity *e.g.*, antimicrobial, anti-cancer, anti-inflammatory, antimalarial, antiallergic, antioxidant, anti-infective, anti-influenzas, anti-protozoal[12,13] etc. Nevertheless their application as corrosion inhibitors for aluminium in acid media remains outstanding and still ongoing.

The inhibitive properties of three chalcone derivatives on the corrosion rate of aluminum have been experimentally investigated by Fouda *et al.*[14] The aim of this work is to correlate the molecular structure of three chalcone compounds (Fig. 1) and their corresponding corrosion inhibiting effect for aluminium in acid solution (1M phosphoric acid) using some quantum chemical parameters such as E_{HOMO} (highest occupied molecular orbital energy), E_{LUMO} (lowest unoccupied molecular orbital energy), hardness (η), polarizability <α>, molecular volume (MV), dipole moment (μ). Also, the local reactivity has been studied through the Fukui indices in order to predict the possible sites of nucleophilic and electrophilic attacks.

COMPUTATIONAL DETAILS

1. Quantum chemical calculation

The quantum chemical calculations were performed with ORCA program (version 4.1.2).[15] The geometries of the molecules were fully optimized with DFT[16] using Becke's three parameter exchange functional, the Lee-Yang-Parr correlation functional (B3LYP)[17] and, to include the long-range correction essential to describe the electron excitations to high orbitals, the hybrid exchange-correlation functional (CAM–B3LYP) proposed by Yanai *et al.*[18] and the ωB97X-D3 functional proposed by Iikura *et al.*[19] were used. The CAM–B3LYP functional is a hybrid functional with an improved long-range properties, and the ωB97X-D3 functional includes empirical dispersion. These functions were applied with the def2-TZVPP basis set.[20]

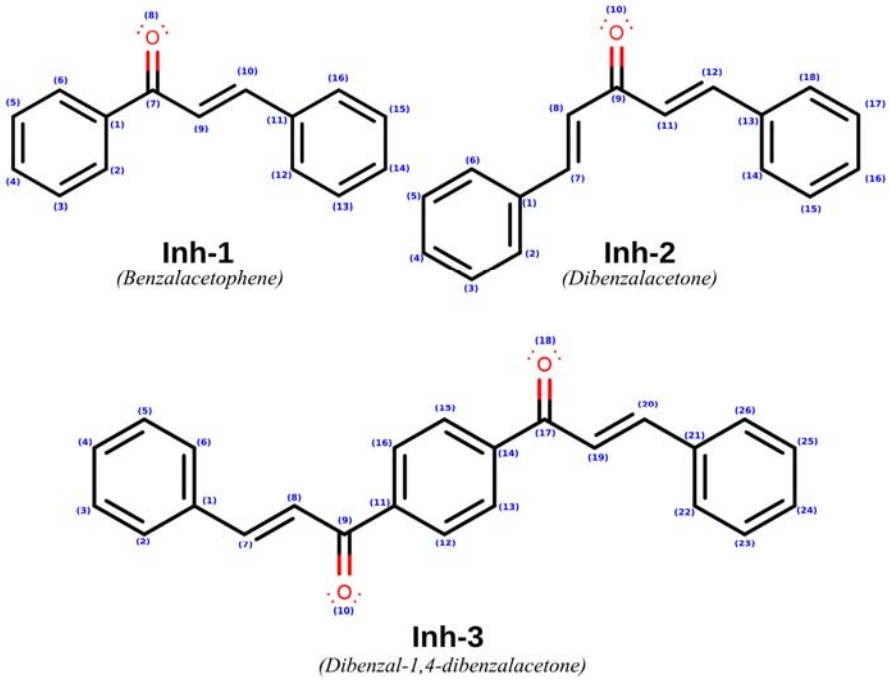

Fig. 1 – Molecular structures of the studied chalcone derivatives.

In addition, the positive and negative regions for the three tested inhibitors were identified from the Electrostatic Potential (ESP) maps and analyzed by the Multi wfn program.[21] Therefore, Visual Molecular Dynamics (VMD) software[22] is used to visualize and analyze the ESP results.

Quantum chemical indices like: the energy of the highest occupied molecular orbital (E_{HOMO}), the energy of the lowest unoccupied molecular orbital (E_{LUMO}), energy gap ($\Delta E_{gap} = E_{LUMO} - E_{HOMO}$), hardness (η), softness (σ), electronegativity (χ), number of transferred electron (ΔN) and Mulliken charges were computed.

The ionization energy (I) and the electron affinity (A) were calculated according to the Koopmans' theorem by the values of the energies of the orbital E_{HOMO} and E_{LUMO} as follows.[23-25]

$$I = - E_{HOMO} \quad (1)$$

$$A = - E_{LUMO} \quad (2)$$

$$\Delta E_{gap} = E_{LUMO} - E_{HOMO} \quad (3)$$

The electronegativity (χ), which measures the power of an atom or group of atoms to attract electrons towards itself can then be written as the average of ionization potential (I) and electron affinity (A)[26]:

$$\chi = \frac{I + A}{2} \quad (4)$$

The hardness of a molecule (η) expresses the resistance of an atom to a charge transfer, it is related to the energy gap between the HOMO and LUMO orbitals. The larger the HOMO-LUMO energy gap the harder will be the molecule. It can be calculated as follows:[27]

$$\eta = \frac{I - A}{2} \quad (5)$$

The inverse of the global hardness is the global softness (σ). It measures the capacity of an atom or a group of atoms to accept electrons it can be calculated by equation (6):[28-30]

$$\sigma = \frac{1}{\eta} = \frac{2}{I - A} \quad (6)$$

The global electrophilicity index ω introduced by Parr *et al.*,[31] measures the tendency of molecules to accept electrons. A good nucleophile is characterized by a low value of ω whereas a good electrophile is characterized by a high value of ω.[29,32] It is defined by the equation Eq. (7).

$$\omega = - \frac{\mu^2}{2\eta} \quad (7)$$

where μ represents the chemical potential and is assumed to be equal to the negative of electronegativity (χ).

The amount of transferred charge ΔN, from the inhibitors to the metal surface was estimated using the Pearson method through the equation bellow:[33-35]

$$\Delta N = \frac{(\chi_M - \chi_{mol})}{2(\eta_M + \eta_{mol})} = \frac{(\pi_{mol} - \pi_M)}{2(\eta_M + \eta_{mol})} \quad (8)$$

Herein χ_M and χ_{mol} represent the absolute electronegativity of the metal and the inhibitor, respectively. η_M and η_{mol} are the absolute hardness of the metal and the inhibitor, respectively. The electron transfer is governed by the difference in electronegativities, while the sum of the hardness parameters acts as a resistance. In this study, we used the theoretical values χ_M = 3.23 eV and η_M = 0 eV for aluminium, according to R.G. Pearson.

The electric dipole polarizability is inversely proportional to the third power of the hardness value.[26] The following equation is used.

$$< \alpha > = \left(\frac{\partial^2 E}{\partial^2 F_a \, \partial^2 F_b} \right) a, b = x, y, z \quad (9)$$

The mean polarizability is calculated through the equation Eq. (10):

$$< \alpha > = \frac{1}{3} (\alpha_{xx} + \alpha_{yy} + \alpha_{zz}) \quad (10)$$

Reports in the literature have been focused on the ability of the inhibitor molecule to donate and accept electrons by using others chemical descriptors, such as the electro-donating power (ω^-), electro-accepting (ω^+) power,[36] net electrophilicity ($\Delta\omega^{\pm}$)[37] and back-donation ($\Delta E_{back\text{-}d}$) energy[38] can be calculated following the equations (11) to (14):

$$\omega^- = \frac{(3I + A)^2}{16(I - A)} \quad (11)$$

$$\omega^{+} = \frac{(I + 3A)^2}{16(I - A)} \quad (12)$$

$$\Delta\omega^{\pm} = \{\omega^{+} - (-\omega^{-})\} \text{ or } \Delta\omega^{\pm} = \left\{\omega^{+} - \left(\frac{1}{\omega^{-}}\right)\right\} \quad (13)$$

$$\Delta E_{back-d} = -\frac{\eta}{4} \quad (14)$$

The local reactivity has been analyzed by Fukui function which is an indication of the reactive centers within the molecules. With respect to a finite difference approximation, the condensed Fukui functions were calculated as an atom k in a molecule with N electrons with the expression below:[39]

$$f_K^{+} = q_K(N+1) - q_K(N) \text{ (for nucleophilic attack)} \quad (15)$$

$$f_K^{-} = q_K(N) - q_K(N-1) \text{ (for electrophilic attack)} \quad (16)$$

where $q_k(N - 1)$, $q_k(N + 1)$, $q_k(N)$ are the charges of the cationic, anionic and neutral molecule, respectively. Here Fukui functions are presented through the finite difference approximation using Muliken's population analysis. Morrel *et al*. have proposed a new dual descriptor Δf(r) for nucleophilicity and electrophilicity. It is defined as the difference between the nucleophilic and electrophilic Fukui functions and is given by the equation (17):[40-43]

$$\Delta f(r) = [f_k^{+} - f_k^{-}] \quad (17)$$

If $\Delta f(r) > 0$, then the site is electrophilic, if $\Delta f(r) < 0$, then the site is nucleophilic.

RESULTS AND DISCUSSION

1. Quantum chemical study of the neutral inhibitors

1.1. Global reactivity descriptors

The computed quantum chemical parameters were used, to determine the relationship between chalcone inhibitors and their corresponding inhibition efficiency. The optimized structures, HOMO (highest occupied molecular orbital) and LUMO (lowest unoccupied molecular orbital) are shown in Fig. 2. Additional quantum chemical parameters such as the energy of the highest occupied molecular orbital (E_{HOMO}), the energy of the lowest unoccupied molecular orbital (E_{LUMO}), energy gap (ΔE_{gap}) and dipole moment (μ) were obtained and presented in Table 1.

Molecular orbital theory is a powerful and a useful method; in predicting adsorption centers of the inhibitor molecules over a metal surface. The adsorption process is controlled by donor-acceptor mechanism between chalcone inhibitors and the Aluminium surface. The HOMO electron density supplies data about which part of the inhibitor molecule could easily donate electrons to the proper vacant metal orbitals. The LUMO electron density, on the other hand, reveals the potential sites that are prone to electron acceptance from the appropriate occupied orbitals of the metal.[28,33,42-44] The HOMO surfaces of the three chalcones are of the π-type and they are distributed over the entire molecule, with main focus on the phenyl ring adjoining the double bond and the carbonyl group, respectively. This observation establishes the possibility that the studied chalcones adsorb in the parallel orientation to the aluminium surface, involving the π-electrons of the aromatic ring. The LUMO surfaces shows contributions from phenyl π*-orbital, π*-orbital double bond as well as π*-orbital of the carbonyl group.

From the parameters listed in Table 1 it is observed that the E_{HOMO} for the investigated compounds follow the order: Inh-2 > Inh-1 > Inh-3 which is not in agreement with the experimental inhibition efficiency order. The sequence of the E_{LUMO} values follows the order: Inh-1 > Inh-2 > Inh-3, which is in perfect agreement with the experimental findings.[14] In addition to E_{HOMO} and E_{LUMO}, energy gap (ΔE_{gap}) is another important parameter for explaining surface adsorptive behaviour of the inhibitor molecules. Generally, lower the ΔE_{gap} value higher is the reactivity of the molecules, since the energy to remove an electron from the last occupied orbital will be minimized. Hence, it enhances its adsorption effectively onto the

metallic surfaces.[44,45] The calculated ΔE_{gap} values of the chalcone inhibitors lies in the order of Inh-3 > Inh-2 > Inh-1, which is in well accordance with the results obtained from the experimental data.[14]

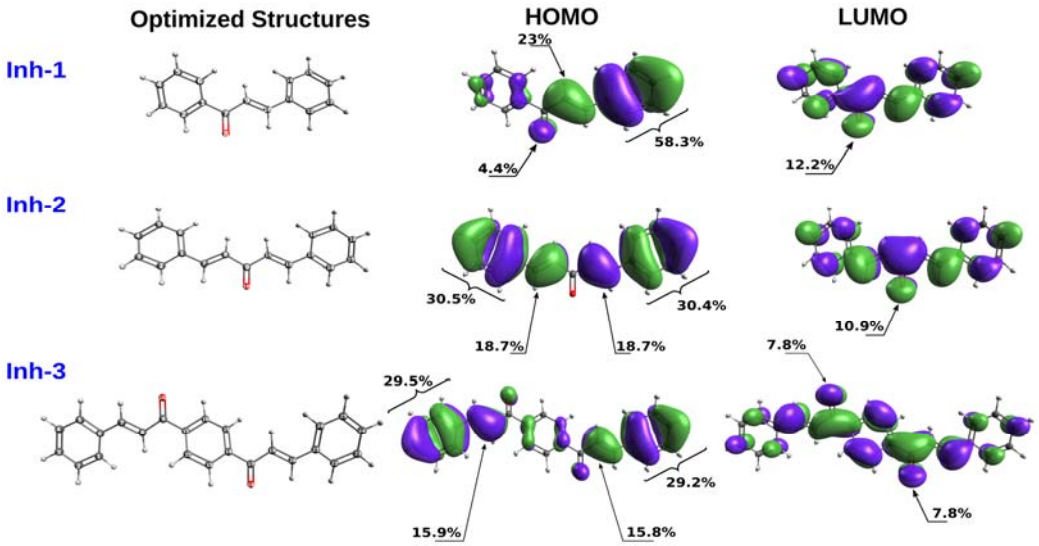

Fig. 2 – The optimized structures, HOMO and LUMO for the investigated inhibitors, Inh-1, Inh-2 and Inh-3 at CAM-B3LYP/def2-TZVPP level.

Table 1

Calculated quantum chemical descriptors [(i)] of the three chalcone inhibitors at CAM-B3LYP/ωB97X-D3 functionals combined with def2-TZVPP basis set, and the measured average inhibition efficiencies IE (%)

Parameters	**Molecules**		
	Inh-1	**Inh-2**	**Inh-3**
HOMO (eV)	-7,996 / -8,775	-7,855 /-8,627	-8,004 /-8,784
LUMO (eV)	-1,374 / -0,592	-1,629 / -0,854	-1,794 /-1,031
ΔE_{gap} (eV)	6,622 / 8,184	6,226 / 7,773	6,21 /7,754
I (eV)	7,996 / 8,775	7,855 / 8,627	8,004 /8,784
A (eV)	1,374 / 0,592	1,629 / 0,854	1,794 /1,031
μ (Debye)	4,779 / 4,684	4,576 / 4,468	0,009 /0,009
< α > (a.u.)	270,04 / 267,40	330,66 / 324,75	453,06 /446,76
V^{vdw} (Bohr^3)	1762,57 / 1762,54	2011,47 /2011,44	2794,10 /2793,99
SA (Bohr^2)	924,84 /924,81	1056,04 /1056,02	1418,48 /1418,34
TE (a.u.)	-653,93 / -654,09	-731,32 / -731,50	-1075,66 /-1075,92
χ	4,685 / 4,684	4,742 / 4,741	4,899 /4,907
π	-4,685 / -4,684	-4,742 / -4,741	-4,899 /-4,907
η	3,311 / 4,092	3,113 / 3,887	3,105 /3,877
σ	0,302 / 0,244	0,321 / 0,257	0,322 /0,258
ω	3,315 / 2,68	3,611 / 2,891	3,865 /3,106
ω^-	6,071 / 5,534	6,371 / 5,747	6,703 /6,044
ω^+	1,386 / 0,85	1,629 / 1,007	1,804 /1,137
$\Delta\omega^{\pm}$	7,457 / 6,384	8.000 / 6,754	8,507 /7,181
$\Delta\omega^{\pm}$	1,221 / 0,669	1,472 / 0,833	1,655 /0,971

Table 1 (continued)

ΔN	-0,223 / -0,18	-0,246 / -0,197	-0,272 /-0,219
Δn_{back-d}	-0,828 /-1,023	-0,778 / -0,972	-0,776 /-0,969
IE%[14]	**45.6**	**57.1**	**64.8**

(i): Energies of highest occupied molecular orbital (E_{HOMO}); Energies of lowest unoccupied molecular orbital (E_{LUMO}); Energy gap (ΔE_{gap}); Ionization potential (I); Electron affinity (A); Dipole moment (μ); Polarizability <α>; Total energy (TE); Electronegativity (χ); Chemical potential (π); Global hardness (η); Global softness (σ); Global Electrophilicity (ω); electro-donating power (ω^-); electro-accepting power (ω^+); net electrophilicity (Δω±) and back-donation (ΔE_{back-d}).

The dipole moment μ is widely used as a reactivity parameter; it results from the non-uniform distribution of charges on atoms in the molecule. It provides information on the polarity of the whole molecule. Though many authors state that low values of dipole moment favours accumulation of the inhibitor molecule in the surface layer and therefore higher inhibition efficiency. According to the literature survey the correlation between the dipole moment and the inhibition efficiency reveals many irregularities. So, in general, there is no significant relationship between dipole moment values and inhibition efficiencies.[28,35,42,46] In the present study, the results suggest that the inhibition efficiencies (IE%) increases as the values of the dipole moment **μ** decreases.

The number of electrons transferred ΔN, measures the ability of a chemical compound to transfer its electrons to a metal if $\Delta N > 0$, and vice versa if $\Delta N < 0$.[26,46-48] In this study, the negative values of ΔN presented in Table 1, suggest the high capability of the chalcone inhibitors to accept electrons from aluminum surface. A back-donating bond can be formed between the anti-bonding aluminium orbitals and the inhibitor molecule.

Another important indices to elucidate the inhibiting behavior of the studied chalcones on the aluminum surface, are the **absolute hardness (η) and softness (σ).** The chemical hardness represents essentially the resistance towards the deformation or polarization of an electronic cloud under a small perturbation of chemical reaction. A hard molecule has a high value of hardness (hence a low value of softness) shows lower reactivity and greater stability. According to Hard and Soft Acids Bases (HSAB) Pearson principle, metals are considered as soft acids and inhibitor molecules as soft bases.[28,44,48,49] Hence, soft–soft interaction is the major controlling factor for the adsorption of the inhibitor molecules. Table 1 reveals that the softness values of the tested chalcones follow the order: Inh-3 > Inh-2 > Inh-1, which is in perfect agreement with the experimental inhibition effectiveness.[14]

The electrophilicity index ω is an important descriptor that measures the ability of a molecule to accept electrons.[3] A high value of ω depicts a good electrophile while a small value of ω indicates a good nucleophile. In our study, Inh-3 exhibits the highest value of electrophilicity ω = 3.865, which confirms its high capacity to accept electrons from the Aluminium surface and a better corrosion inhibition efficiency EI = 64.8 %.[14]

The polarizability α is the ratio of induced dipole moment to the intensity of the electric field. The induced dipole moment is proportional to polarizability and reactivity indication.[26] High values of polarizability facilitate the strong adsorption process of corrosion inhibitors onto the metal surface and hence, high inhibition efficiency. The polarizabilities were evaluated using Eq. (10) for all inhibitors. As can be seen from Table 1, the polarizabilities are in the order Inh-3 > Inh-2 > Inh-1, which correlates well with the observed experimental corrosion inhibition efficiencies.[14]

The Molecular volume (V^{vdw}) and **Surface area (SA)** illustrate possible metal surface coverage by the inhibitor. The corrosion rates decreases as volume and surface area of the molecules increases. A compound with large values has the highest surface coverage and hence might give a very high protection to the metal surface. A comparison of the values for V^{vdw} and SA shows the order Inh-3 > Inh-2 > Inh-1, which is in accordance with the experimentally determined inhibition efficiencies.[14]

1.2. Local reactivity

The local reactivity can be analysed through atomic charges and condensed Fukui functions,[1,50]

in order to ascertain the role of individual atoms in the molecule on the basis of its distinct chemical behaviour.

The Mulliken and natural population analysis (NPA) charges have been widely used to estimate the possible adsorption centers of the inhibitor molecules. Many authors agree that the more an atom or a region is negatively charged, the greater is its tendency to donate electrons and get adsorbed on the metal surface through a donor–acceptor interaction type.[49] The calculated charge distributions using Mulliken and natural population analysis (NPA) are tabulated in Table 2.

As it can be seen from Table 2 for the calculated charges values, oxygen atom of the carbonyl group (O8, O10 and O10, O19 for Inh-1, Inh-2 and Inh-3 molecules, respectively) present a considerable excess of negative charge in both NPA and Mulliken methods. Therefore, the more negative atomic charges indicated that oxygen atom of the carbonyl group is the most active adsorption site for the three tested inhibitors.

The f_k^+ measures the changes of density when the molecules gains electrons and it corresponds to reactivity with respect to nucleophilic attack. On the other hand f_k^-, corresponds to reactivity with respect to electrophilic attack or when the molecule loses electrons.[26,30,42,51]

The calculated Fukui indices (f_k^+ and f_k^-) for the three chalcone inhibitors, using Mulliken population analysis, have been determined and presented in Fig. 3, in which only the highest values are illustrated. All calculated values for all atoms are given as supplementary data (Tables S1-S3).

Table 2

Calculated atomic charges (Muliken and natural population analysis (NPA)) for the tested chalcones at CAM-B3LYP/def2-TZVPP

Inh-1			Inh-2			Inh-3		
Atom	**Mulliken**	**NPA**	**Atom**	**Mulliken**	**NPA**	**Atom**	**Mulliken**	**NPA**
C1	0,012	-0,160	**C1**	0,047	-0,106	**C1**	0,016	-0,109
C2	-0,178	-0,177	**C2**	-0,186	-0,184	**C2**	-0,167	-0,182
C4	-0,147	-0,188	**C4**	-0,137	-0,200	**C4**	-0,154	-0,197
C5	-0,174	-0,221	**C5**	-0,184	-0,220	**C5**	-0,171	-0,220
C6	-0,178	-0,167	**C6**	-0,177	-0,179	**C6**	-0,159	-0,176
C7	0,289	0,540	**C7**	-0,055	-0,084	**C7**	-0,033	-0,070
O8	**-0,400**	**-0,618**	**C8**	-0,159	-0,321	**C8**	-0,171	-0,334
C9	-0,174	-0,329	**C9**	0,247	0,508	**C9**	0,262	0,538
C10	-0,027	-0,077	**O10**	**-0,421**	**-0,638**	**O10**	**-0,391**	**-0,610**
C11	0,022	-0,107	**C11**	-0,172	-0,321	**C11**	0,010	-0,128
C12	-0,160	-0,178	**C12**	-0,056	-0,084	**C12**	-0,166	-0,169
C13	-0,176	-0,219	**C13**	0,038	-0,106	**C13**	-0,138	-0,179
C14	-0,146	-0,199	**C14**	-0,165	-0,183	**C14**	0,010	-0,128
C15	-0,185	-0,216	**C15**	-0,197	-0,216	**C15**	-0,166	-0,169
C16	-0,176	-0,183	**C16**	-0,146	-0,200	**C16**	-0,138	-0,179
			C17	-0,173	-0,220	**C17**	0,263	0,538
			C18	-0,176	-0,179	**O18**	**-0,391**	**-0,610**
						C19	-0,171	-0,333
						C20	-0,032	-0,070
						C21	0,015	-0,109
						C22	-0,159	-0,176
						C23	-0,171	-0,220
						C24	-0,154	-0,197
						C25	-0,180	-0,215
						C26	-0,167	-0,182

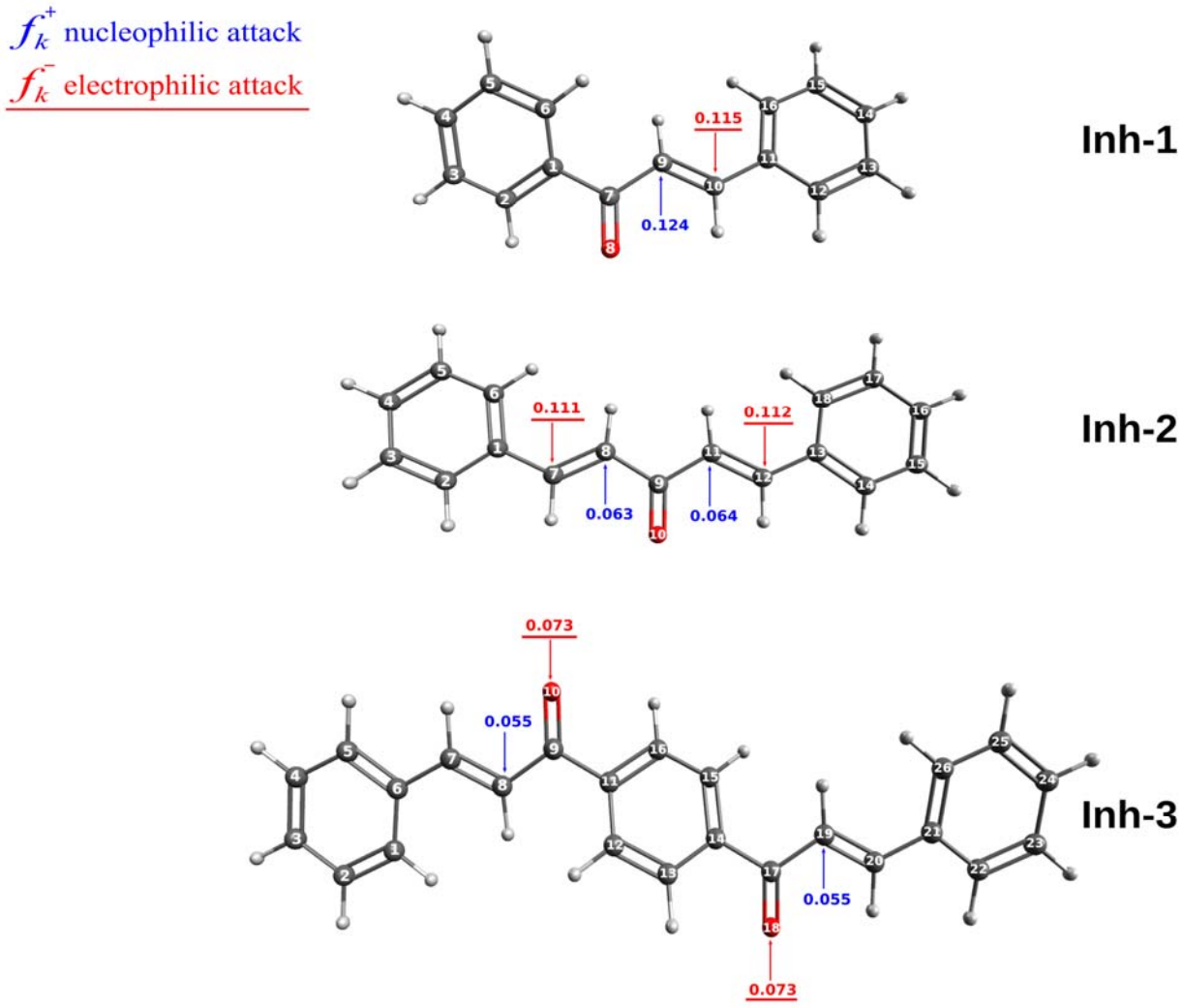

Fig. 3 – Condensed Fukui functions (f_k^+ and f_k^-) on the selected atoms for the studied chalcone derivatives at CAM-B3LYP/def2-TZVPP level.

The preferred site for a nucleophilic attack, shown by the highest value of f_k^+ is on the α carbon to the carbonyl group for all the inhibitor molecules. Atom (C9: 0.124): Inh-1, atoms (C8:0.063) and (C11, 0.0642): Inh-2, and atoms (C8:0.055), (C19:0.055) for Inh3. While the highest values f_k^- of are localised on the β carbon to the carbonyl group for Inh-1 and Inh-2: C(10), C(7) and C(12) with values 0.0115 and 0.111 and 0.112 respectively. For Inh-3 the f_k^- are located on the oxygen atoms: O(10) and O(18) with 0.073 value for both atoms. The results obtained from nucleophilic and electrophilic site determination support the ability of the chalcone molecules to react with aluminium surface through donor-acceptor interaction.

However, the minima and maxima of the molecular electrostatic potential (ESP) are shown in blue and red colors, respectively (see Fig. 4), are associated with the sites of electrophilic and nucleophilic attacks.

As can be seen from Fig. 4, the most negative area (blue sites) are located predominantly around the oxygen atom of the carbonyl group for the three tested inhibitors, with the values of -49.47, -52.01 and -45.01 kcal/mol, respectively for the Inh-1, Inh-2 and Inh-3. It also can be observed, that the blue regions are located at the center of the aromatic rings for the three inhibitors.

This result indicates that not only the oxygen atom of the carbonyl groups are the most favorable sites for electrophilic attacks, but also the phenyl rings for the three inhibitors serve as reactive centers for the adsorption on the metallic surface, and consequently suggesting a possible interactions with a preferring parallel orientation.

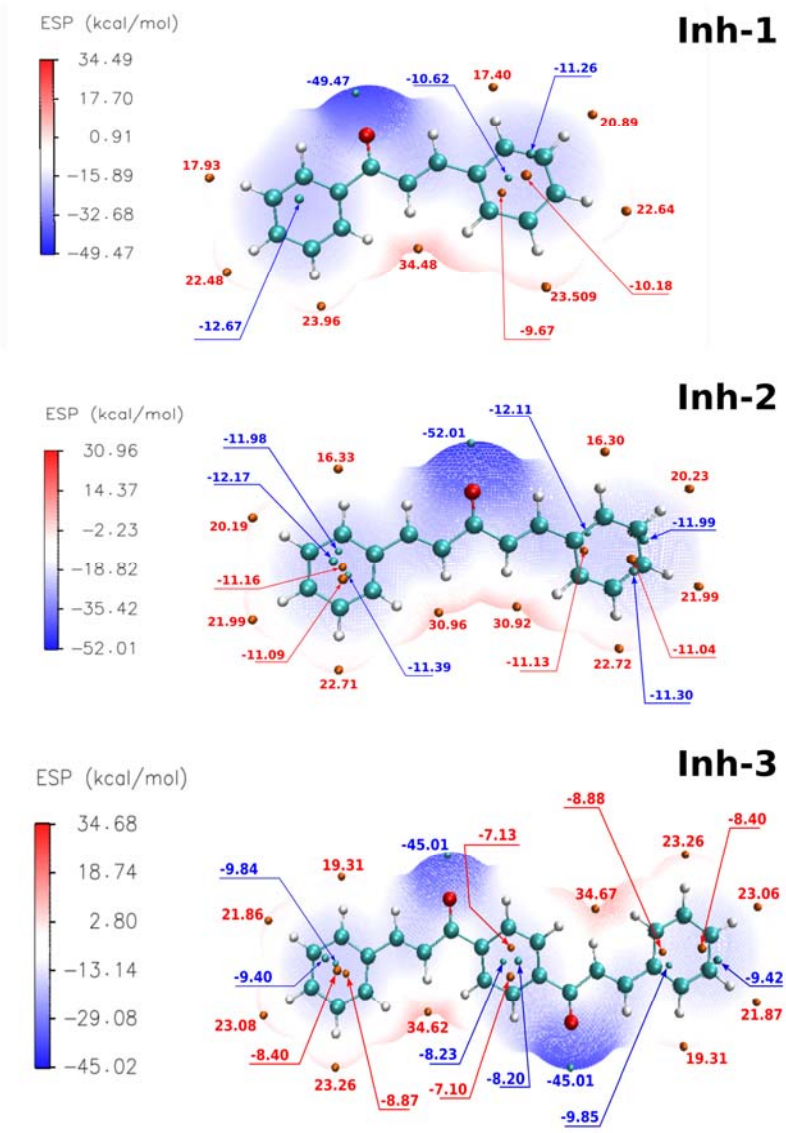

Fig. 4 – Electrostatic potential (ESP) mapped molecular VDW surface of the three tested inhibitors.

3.2. Protonated forms

In a strong acid solutions such as phosphoric acid (H_3PO_4, 1M), chalcone compounds are expected to be protonated. The calculations show a great stability of the protonated inhibitors. The neutral inhibitors (Fig. 3), show one or more reactive site. In order to find the most suitable protonation site, optimization of all possible structures with different protonated centers was carried out and it was found that the most possible one with lowest energy upon the protonation was O(8) atom for Benzalacetophene, O10 atom for Dibenzalacetone and O10 for Dibenzal-1, 4-Dibenzalacetonerespectively.

The optimized geometries of Inh-1-H^+, Inh-2-H^+ and Inh-3-H^+ in the protonated form including their HOMO and LUMO distributions are displayed in Fig. 5.

A comparison of the quantum chemical calculations between the neutral and protonated form of the inhibitors reveals that there is an excellent correlation between the most significant descriptors (ΔE_{gap}, η, σ, ΔN) of the protonated form of the inhibitors and the inhibition efficacy (Table 1 and Table 3). The results obtained from the protonated form are in perfect agreement with the experimental inhibition efficiency: Inh-1 < Inh-2 < Inh-3.

These results state that in an acid medium, the protonated form of the inhibitors has a higher contribution to the corrosion inhibiting effect on the aluminum surface.

Table 3

Calculated quantum chemical descriptors [(i)] of the chalcone derivatives studied at CAM-B3LYP functional combined with def2-TZVPP basis set and the measured average inhibition efficiencies IE (%) in the protonated forms

Parameters	**Molecules**		
	Inh1-H$^+$	**Inh2-H$^+$**	**Inh3-H$^+$**
HOMO (eV)	-8.447	-8.092	-8.096
LUMO (eV)	-2.743	-2.890	-2.925
I (eV)	8.447	8.092	8.096
A (eV)	2.743	2.890	2.925
ΔE_{gap} (eV)	5.704	5.202	5.172
μ (Debye)	4.009	2.819	15.122
< α > (a.u.)	316.386	421.162	507.074
V^{vdw} (Bohr^3)	1767.80	2018.48	2803.06
SA (Bohr^2)	926.60	1055.92	1418.04
TE (a.u.)	-654.36	-731.75	-1076.09
χ	5.595	5.491	5.510
π	-5.595	-5.491	-5.510
η	2.852	2.601	2.586
σ	0.351	0.384	0.387
ω	5.488	5.796	5.871
ω^-	8.642	8.867	8.950
ω^+	3.047	3.376	3.439
Δω	11.690	12.243	12.389
Δω	2.932	3.263	3.328
ΔN	-0.418	-0.439	-0.445
$\Delta E_{back\text{-}d}$	-0.713	-0.650	-0.646
IE%[14]	**45.6**	**57.1**	**64.8**

[(i)] Chemical descriptors exposed in the legend of Table 1.

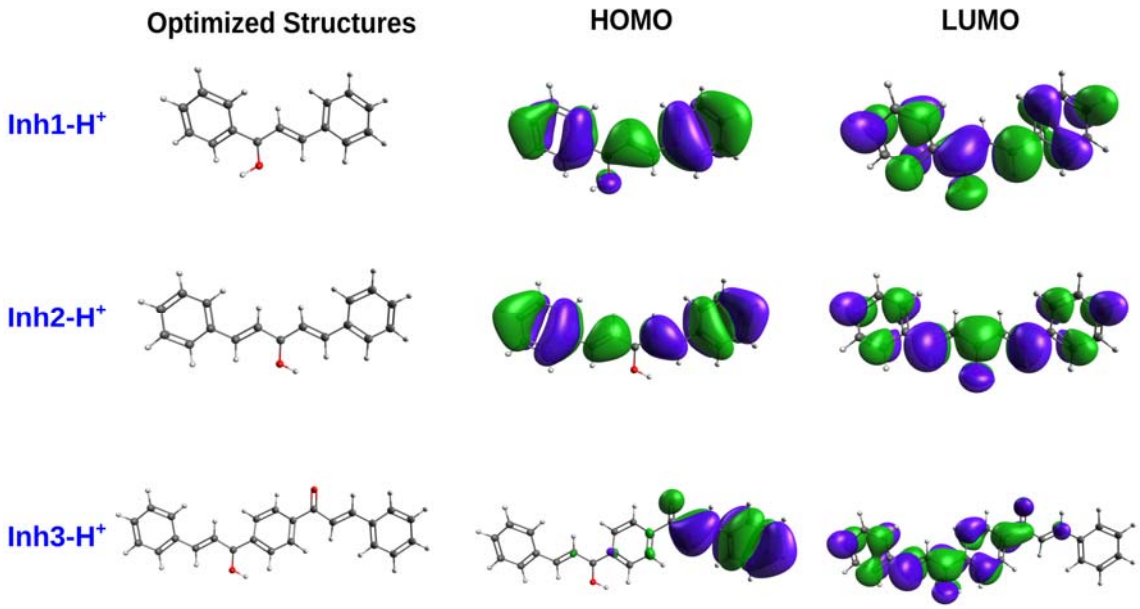

Fig. 5 – Optimized structures, HOMO and LUMO of the chalcone derivatives studied at CAM-B3LYP/def2-TZVPP level in the protonated forms.

CONCLUSIONS

The inhibition effectiveness of Aluminum corrosion in 1M phosphoric acid by three chalcone derivatives has been investigated using quantum chemical calculations based on density functional theory at CAM-B3LYP/ωB97X-D3 functional combined with def2-TZVPP basis set level.

The calculated electronic parameters involved in the inhibition confirmed that the order of the inhibition efficiency increases with the decrease in E_{LUMO}, and energy gap (ΔE_{gap}). Inh-3 has the highest inhibition efficiency, EI = 64.8%.

The density distributions of the frontier molecular orbitals (HOMO and LUMO) show that chalcone compounds adsorb through π electrons of the phenyl ring, double bond and oxygen heteroatom.

The parameters like hardness, softness, electron affinity, ionization potential, electronegativity, dipole moment, polarizability and the fraction of electron transferred confirm the experimental inhibition efficiencies order: Inh-3 > Inh-2 > Inh-1.

The Fukui indices for the studies chalcone molecules describe well the nucleophilic and electrophilic sites responsible for electron donation and acceptance.

REFERENCES

1. B. G. Prakashaiah, D. Vinaya Kumara, A. Anup Pandith, A. Nityananda Shetty and B. E. Amitha Rani, *Corros. Sci*., **2018**, *136*, 326-338. https://doi.org/10.1016/j.corsci.2018.03.021.
2. R. M. Hassan, S. M. Ibrahim, H. D. Takagi and S. A. Sayed, *Carbohydr. Polym*., **2018**, *192*, 356-363. https://doi.org/10.1016/j.carbpol.2018.03.066.
3. U. J. Naik, P. C. Jha, M. Y. Lone, R. R. Shah and N. K. Shah, *J. Mol. Struct*., **2016**, *1125*, 63-72. https://doi.org/10.1016/j.molstruc.2016.06.054.
4. X. Y. Zhang, Q. X. Kang and Y. Wang, *Comput. Theor. Chem*., **2018**, *1131*, 25-32. https://doi.org/10.1016/j.comptc.2018.03.026.
5. M. Dibetsoe, L. Olasunkanmi, O. Fayemi, S. Yesudass, B. Ramaganthan, I. Bahadur, A. Adekunle, M. Kabanda and E. Ebenso, *Molecules*, **2015**, *20*, 15701-15734. https://doi.org/10.3390/molecules200915701.
6. M. Abdallah, E. M. Kamar, S. Eid and A. Y. El-Etre, *J. Mol. Liq*., **2016**, *220*, 755-761. https://doi.org/10.1016/j.molliq.2016.04.062.
7. T. M. A. Al Shboul, T. M. A. Jazzazi and T. T. Bataineh, *Jordan J. Chem*., **2014**, *9*, 149-158. https://doi.org/10.12816/0026397.
8. A. El Nemr, A. A. Moneer, A. Khaled, A. El Sikaily and G. F. El-Said, *Mater. Chem. Phys*., **2014,** *144*, 139-154. https://doi.org/10.1016/j.matchemphys.2013.12.034.
9. Q. X. Kang, Y. Wang and X. Y. Zhang, *J. Alloys Compd*., **2019**, *774*, 1069-1080. https://doi.org/10.1016/j.jallcom.2018.09.391.
10. P. Singh, M. A. Quraishi, E. E. Ebenso and C. B. Verma, *Int. J. Electrochem. Sci*., **2014**, *9*, 7446 – 7459.
11. J. R. Almeida, J. Moreira, D. Pereira, S. Pereira, J. Antunes, A. Palmeira, V. Vasconcelos, M. Pinto, M. Correia-da-Silva and H. Cidade, *Sci. Total Environ*., **2018**, *643*, 98–106. https://doi.org/10.1016/j.scitotenv.2018.06.169.
12. A. M. Maharramov, Y. V. Mamedova, M. R. Bayramov and I. G. Mamedov, *Russ. J. Phys. Chem. A*., **2018**, *92*, 2154–2158. https://doi.org/10.1134/ S0036024418110250.
13. S. Velrani and R. Mahalakshmi, *RASAYAN J. Chem*., **2015**, *8*, 156-160.
14. A. S. Fouda, M. Abdallah and M. Eissa, *Afr. J. Pure Appl. Chem*., **2013**, *7*, 394-404. DOI:10.5897/AJPAC2013.0534.
15. F. Neese, *WIREs Comput. Mol. Sci.*, **2018**, 8. https://doi.org/10.1002/wcms.1327.
16. A. D. Becke, *J. Chem. Phys*., **1986,** *84*, 4524–4529. https://doi.org/10.1063/1.450025.
17. A. D. Becke, *J. Chem. Phys*., **1993**, *98*, 5648–5652. https://doi.org/10.1063/1.464913.
18. T. Yanai, D. P. Tew and N. C. Handy, *Chem. Phys. Lett*., **2004**, *393*, 51–57. https://doi.org/10.1016/j.cplett.2004.06.011.
19. Y.-S. Lin, G.-D. Li, S.-P. Mao and J.-D. Chai, *J. Chem. Theory Comput.*, **2013**, *9*, 263–272. https://doi.org/10.1021/ct300715s.
20. F. Weigend and R. Ahlrichs, *Phys. Chem. Chem. Phys.*, **2005**, *7*, 3297–3305. https://doi.org/10.1039/b508541a.
21. T. Lu and F. Chen, *J. Comput. Chem*., **2012**, *33*, 580-592.
22. W. Humphrey, A. Dalke and K. Schulten, *J. Mol. Graph.*, **1996**, *14*, 33-38.
23. A. Fiala, W. Boukhedena, S. E. Lemallem, H. Brahim Ladouani and H. Allal, *J. Bio- Tribo-Corros*., **2019**, *5*, 42. https://doi.org/10.1007/s40735-019-0237-5.
24. S. E. Hachani, Z. Necira, D. E. Mazouzi and N. Nebbache, *Acta Chim. Slov*., **2018,** *65*, 183-190. https://doi.org/10.17344/acsi.2017.3803.
25. A. Zarrouk, H. Zarrok, R. Salghi, B. Hammouti, S. S. Al-Deyab, R. Touzani, M. Bouachrine, I. Warad and T. B. Hadda, *Int. J. Electrochem. Sci.*, **2012**, *7*, 6353 – 6364.
26. M. Shahraki, M. Dehdab and S. Elmi, *J. Taiwan Inst. Chem. Eng*., **2016**, *62*, 313-321. https://doi.org/10.1016/j.jtice.2016.02.010.
27. N. Ammouchi, H. Allal, Y. Belhocine, S. Bettaz and E. Zouaoui, *J. Mol. Liq*., **2020**, *300*, 112309.https://doi.org/10.1016/j.molliq.2019.112309.
28. N. A. Wazzan, *J. Ind. Eng. Chem.*, **2015**, *26*, 291-308. https://doi.org/10.1016/j.jiec.2014.11.043.
29. H. M. A. El-Lateef, M. S. S. Adam and M. M. Khalaf, *J. Taiwan Inst. Chem. Eng*., **2018**, *88*, 286-304. https://doi.org/10.1016/j.jtice.2018.04.024.
30. K. Raja, A. N. Senthilkumar and K. Tharini, *Appl. Sci. Res*., **2016**, *5*, 150-154.
31. A. Srivastava, P. Rawat, P. Tandon and R. N. Singh, *Comput. Theor. Chem*., **2012**, *993*, 80-89. https://doi.org/10.1016/j.comptc.2012.05.025.
32. I. B. Obot, S. Kaya, C. Kaya and B. Tüzün, *Phys. E Low-Dimens. Syst. Nanostructures*., **2016,** *80*, 82-90. https://doi.org/10.1016/j.physe.2016.01.024.
33. Y. Liang, C. Wang, J. Li, L. Wang and J. Fu, *Int. J. Electrochem. Sci*., **2015**, *10*, 8072-8086.

34. H. Allal, Y. Belhocine and E. Zouaoui, *J. Mol. Liq*., **2018**, *265*, 668-678. https://doi.org/10.1016/j.molliq.2018.05.099.
35. N. O. Obi-Egbedi, I. B. Obot and M. I. El-Khaiary, *J. Mol. Struct*., **2011**, *1002*, 86-96. https://doi.org/10.1016/j.molstruc.2011.07.003.
36. J. L. Gázquez, A. Cedillo and A. Vela, *J. Phys. Chem. A.*, **2007**, *111*, 1966–1970. 10.1021 / jp065459f.
37. P. K. Chattaraj, A. Chakraborty and S. Giri, *J. Phys. Chem*., **2009**, *A 113*, 10068–10074. https://doi.org/10.1021/jp904674x.
38. B. Gómez, N. V. Likhanova, M. A. Domínguez-Aguilar, R. Martínez-Palou, A. Vela and J. L. Gázquez, *J. Phys. Chem*., **2006**, *B 110*, 8928–8934. https://doi.org/10.1021/jp057143y.
39. H. Lgaz1, R. Salghi and I. H. Ali, *Int. J. Electrochem. Sci*., **2018**, 250-264. https://doi.org/10.20964/2018.01.26.
40. M. Pandey, S. Muthu and N. M. Nanje Gowda, *J. Mol. Struct*., **2017**, *1130*, 511-521. https://doi.org/10.1016/j.molstruc.2016.10.064.
41. A. Singh, K. R. Ansari, J. Haque, P. Dohare, H. Lgaz, R. Salghi and M. A. Quraishi, *J. Taiwan Inst. Chem. Eng*., **2018**, *82*, 233-251. https://doi.org/10.1016/j.jtice.2017.09.021.
42. N. A. Wazzan and F. M. Mahgoub, *Open J. Phys. Chem*., **2014**, *4*, 6-14. https://doi.org/10.4236/ojpc.2014.41002.
43. X. Li, S. Deng and X. Xie, *J. Taiwan Inst. Chem. Eng*., **2014**, *45*, 1865-1875. https://doi.org/10.1016/j.jtice.2013.10.007.
44. S. Khalil, G. Al-Mazaideh and N. Ali, *Int. J. Biochem. Res. Rev*., **2016**, *14*, 1-7. https://doi.org/10.9734/IJBCRR/2016/29288.
45. I. Danaee, O. Ghasemi, G. R. Rashed, M. Rashvand Avei and M. H. Maddahy, *J. Mol. Struct*., **2013**, *1035*, 247-259. https://doi.org/10.1016/j.molstruc.2012.11.013.
46. S. Kr. Saha, P. Ghosh, A. Hens, N. C. Murmu and P. Banerjee, *Phys. E Low-Dimens. Syst. Nanostructures*, **2015**, *66*, 332-341. https://doi.org/10.1016/j.physe.2014.10.035.
47. H. Lgaz, K. Subrahmanya Bhat, R. Salghi, Shubhalaxmi, S. Jodeh, M. Algarra, B. Hammouti, I. H. Ali and A. Essamri, *J. Mol. Liq*., **2017**, *338*, 71-83. https://doi.org/10.1016/j.molliq.2017.04.124.
48. S. Kr. Saha, M. Murmu, N. C. Murmu, I. B. Obot and P. Banerjee, *Surf. Interfaces*., **2018**, *10*, 65-73. https://doi.org/10.1016/j.surfin.2017.11.007.
49. O. Sikemi, O. A. Kolawole and S. Banjo, J. Mol. Liq.**2017**, 238, 71–83.
50. M. Abdallah, E. A. M. Gad, M. Sobhi, J. H. Al-Fahemi and M. M. Alfakeer, *Egypt. J. Pet*., **2019**, *28*, 173-181. https://doi.org/10.1016/j.ejpe.2019.02.003.
51. R. D. Vargas-Sánchez, A. M. Mendoza-Wilson, R. R. Balandrán-Quintana, G. R. Torrescano-Urrutia and A. Sánchez-Escalante, *Comput. Theor. Chem*., **2015**, *1058*, 21-27. https://doi.org/10.1016/j.comptc.2015.01.014.